Frontiers of Physics
https://doi.org/10.1007/s11467-021-1088-3
Front. Phys.
16(6), 63506 (2021)

RESEARCH ARTICLE

Diverse magnetism in stable and metastable structures of CrTe

Na Kang, Wenhui Wan†, Yanfeng Ge, Yong Liu‡

State Key Laboratory of Metastable Materials Science and Technology & Key Laboratory for Microstructural Material Physics of Hebei Province, School of Science, Yanshan University, Qinhuangdao 066004, China
Corresponding authors. E-mail: †wwh@ysu.edu.cn, ‡yongliu@ysu.edu.cn
Received January 2, 2021; accepted May 12, 2021

In this paper, we systematically investigated the structural and magnetic properties of CrTe by combining particle swarm optimization algorithm and first-principles calculations. By considering the electronic correlation effect, we predicted the ground-state structure of CrTe to be NiAs-type (space group $P6_3/mmc$) structure at ambient pressure, consistent with the experimental observation. Moreover, we found two extra meta-stable $Cmca$ and $R\bar{3}m$ structures which have negative formation enthalpy and stable phonon dispersion at ambient pressure. The $Cmca$ structure is a layered antiferromagnetic metal. The cleaved energy of a single layer is 0.464 J/m^2, indicating the possible synthesis of CrTe monolayer. The $R\bar{3}m$ structure is a ferromagnetic half-metal. When external pressure is applied, the ground-state structure of CrTe transitions from $P6_3/mmc$ structure to $R\bar{3}m$ structure at a pressure of 34 GPa, then to $Fm\bar{3}m$ structure at 42 GPa. We thought these results help to motivate experimental studies of the CrTe compounds in the application of spintronics.

Keywords CrTe, meta-stable structure, antiferromagnetic metal, ferromagnetic half-metal

1 Introduction

The present spintronic devices mainly consist of ferromagnetic (FM) materials, which have shortcomings such as low integration and slow operating frequency [1]. In 2006, antiferromagnetic (AFM) metals are predicted to have giant magnetoresistance [2], which was then observed in the experiment [3]. Antiferromagnets have several advantages in spintronic application, such as high magnetic susceptibility, high switching frequency, the absence of stray fields, and strong spin transfer torque capability [4, 5]. Magnetic transition-metal chalcogenides (TMCs) with rich structural and magnetic properties are regarded as promising candidate materials in spintronics [6–8]. It is significant to explore the unknown FM and AFM structures of TMCs.

Here we focus on the CrTe compounds. On the experimental side, according to the phase diagram determined by Ipser *et al.* [9], the $Cr_{1-\delta}Te$ system has the hexagonal NiAs (NA) structure for $\delta \leq 0.1$. NA CrTe is a FM material with a Curie temperature of 340 K [10]. Furthermore, Wang *et al.* [11] synthesized the film of NA CrTe with a thickness of 11–45 nm and found that it still had a hard magnetism. Apart from the NA structure, a metastable zinc-blende (ZB) CrTe [12] has been grown using molecular-beam epitaxy on GaAs (100) substrate. Eto *et al.* [13] founded that CrTe occurred a structural transition from the NA structure to the MnP (MP) one at pressures between 13 and 14 GPa. Moreover, a $CrTe_3$ compound with a layered structure was synthesized with a long-range AFM order [14], indicating that layered structure may also exist in the CrTe compounds.

On the theoretical side, using the full-potential linear augmented plane waves (FP-LAPWs) method, Charifi *et al.* [15] compared the energy of CrTe in NA, ZB, MP, and Rock-salt (RS) structure, and found that NA structure was the ground state. Dijkstra *et al.* [16] found that NA CrTe had strong Cr 3*d*-Te 5*p* hybridization and the Cr $3d_{z^2}$–Cr $3d_{z^2}$ overlap along the *c* axis. Kanchana *et al.* [17] predicted that NA CrTe had a magnetic transition from FM to non-magnetic (NM) state in around 45.3 GPa utilizing the tight-binding linear muffin-tin orbital method. It was predicted that ZB CrTe had a total energy 0.36 eV higher than the NA CrTe [18]. Block *et al.* [19] founded that ZB CrTe was a half-metal with a bandgap in the minority channel at the Fermi level, due to stronger CrTe covalent bonding than NA CrTe. Liu *et al.* [20] showed that CrTe in RS structure was only marginally unstable against the NA CrTe, and more stable than the ZB CrTe. However, Belkadi [21] recently predicted that the RS structure was the ground-state structure of CrTe by modified Becke-Johnson (MBJ) exchange potential method. Moulkhalwa *et al.* [22] found that the electronic correlation effect had a large influence on the structural and magnetic properties of Cr-based chalcogenides, which has not been well

* arXiv: 2102.02422. This article can also be found at http://journal.hep.com.cn/fop/EN/10.1007/s11467-021-1088-3.

© Higher Education Press 2021

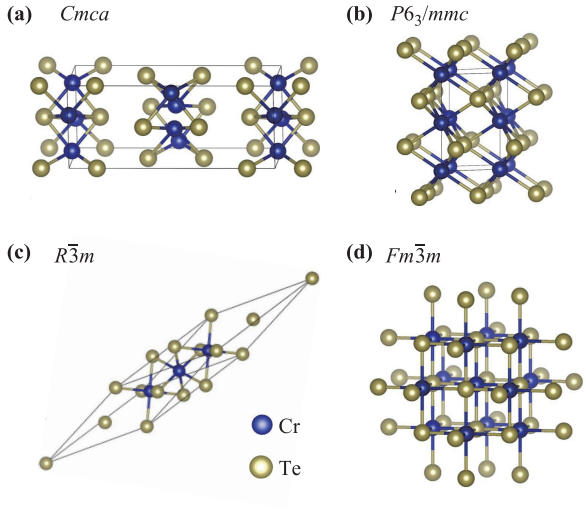

Fig. 1 Crystal lattice of predicted CrTe structures including **(a)** $Cmca$, **(b)** $P6_3/mmc$, **(c)**$R\bar{3}m$, and **(d)** $Fm\bar{3}m$ structures. Blue and brown balls indicate Cr and Te atoms, respectively.

considered in previous calculations.

Considering contradictory results in previous works, in this paper, we investigated the crystal and magnetic structures of CrTe using structure searching technology combined with first-principles calculations. We predicted that the NA structure (space group $P6_3/mmc$) was the ground-state structure by considering the electronic correlation effect. Two extra meta-stable phases including $Cmca$ and $R\bar{3}m$ structures were founded. The $Cmca$ phase has a layered structure and is an AFM metal. The $R\bar{3}m$ phase is a FM half-metal. Their electronic and magnetic properties were carefully analyzed. When the external pressure increases, the ground-state structure of CrTe changes from $P6_3/mmc$ to $R\bar{3}m$ at 34 GPa , and then to $Fm\bar{3}m$ structure at 42 GPa.

2 Methods of computational

The searching of crystal structure was performed by particle swarm optimization algorithm, as implemented in the CALYPSO code [23–25]. Given the chemical composition and external pressure, the atomic arrangement with the global lowest energy on the potential energy surface can be determined [23]. This algorithm has been applied to many systems with reliability [26, 27]. We searched for the low-energy structures of bulk $(CrTe)_n$ with number of formula n from 1 to 4 in the process of the structure prediction. To judge the stability of the CrTe in various structures, we adopted the formation enthalpy (ΔH) that is defined as

$$\Delta H = [h(\mathrm{CrTe}) - h(\mathrm{Cr}) - h(\mathrm{Te})]/2, \quad (1)$$

where 2 is the number of atoms per CrTe formula. The h(CrTe) is the enthalpies per formula corresponding to

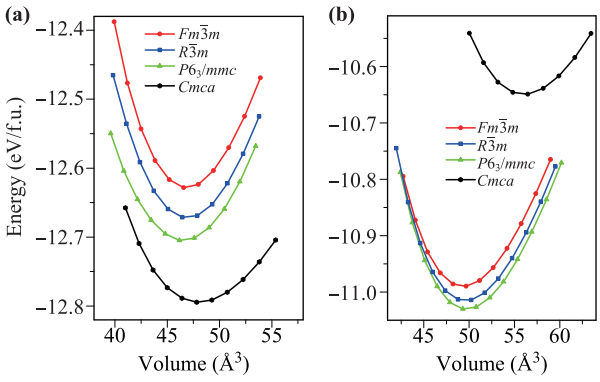

Fig. 2 The energy-volume curves for CrTe in four different phases including $Cmca$, $P6_3/mmc$, $R\bar{3}m$, and $Fm\bar{3}m$ structures by **(a)** PBE and **(b)** PBE+U methods.

the most stable magnetic state of CrTe. h(Cr) and h(Te) are the enthalpy of Cr substance (space group $Im\bar{3}m$) [28] and Te substance (space group $P3_121$) [29], respectively. The first-principles calculations were performed using the Vienna ab initio simulation package (VASP) [30, 31]. The projector augmented wave (PAW) [32] pseudopotentials and Perdew, Burke, and Ernzerhof (PBE) [33] exchange-correlation functionals were used. A plane-wave basis set with an energy cutoff of 500 eV and a monkhorst-Pack [34] k-points with a grid spacing of $2\pi \times 0.08$ Å^{-1} were used. The crystal structures and atomic positions were fully optimized with a force convergence threshold of 0.01 eV/Å. To consider the correlation effects of Cr-d orbitals, we applied the PBE+U scheme [35]. The onsite effective U_f value of Cr-d electrons in CrTe system was determined to be 4 eV (see Fig. S1) by the linear response methods [36]. The phonon spectrum was calculated using density functional perturbation theory [37].

3 Results and discussion

3.1 Meta-stable structures

Calculated formation enthalpies of CrTe compounds, within the chemical compositions available in the experiment [9–14], show that Cr–Te compound with a Cr:Te ratio of 1:1 has the lowest formation enthalpy ΔH (see Fig. S9). Through the structural search at ambient pressure, several structures in CrTe system with a large negative ΔH including $Cmca$, $P6_3/mmc$ (NA), $R\bar{3}m$ and $Fm\bar{3}m$ (RS) structures are predicted (see Fig. 1), while the ZB and MnP structures have much smaller negative ΔH. The energy-volume curve of four low-energy structures are displayed in Fig. 2. Considering the layered structure of the $Cmca$ phase, we adopted the van der Waals (vdw) functional [38] in the first-principles calculations. In PBE calculations, the $Cmca$ structure is the ground-state structure and $P6_3/mmc$ structure is a meta-

Table 1 The space group (SG), group number (GN), the ground magnetic state (MS), lattice parameters (LP), bonding length (d_{CrTe}) and formation enthalpies (ΔH) of CrTe. The numbers of atoms in a conventional cell (N_{cell}) are also given.

SG (GN) N_{cell}	MS	LP (Å, (°))	d_{CrTe} (Å)	ΔH (eV/atom)
$Cmca$ (64)	AFM	$a = 5.743$	2.814	–0.592
16		$b = 12.671$		
		$c = 6.026$		
		$\alpha = \beta = \gamma = 90°$		
$P6_3/mmc$ (194)	FM	$a = b = 4.216$	2.920	–0.782
4		$c = 6.452$		
		$\alpha = \beta = 90°$		
		$\gamma = 120°$		
$R\bar{3}m$ (166)	FM	$a = b = c = 10.184$	2.925	–0.774
6		$\alpha = \beta = \gamma = 23.7°$		
$Fm\bar{3}m$ (225)	FM	$a = b = c = 5.817$	2.909	–0.762
8		$\alpha = \beta = \gamma = 90°$		

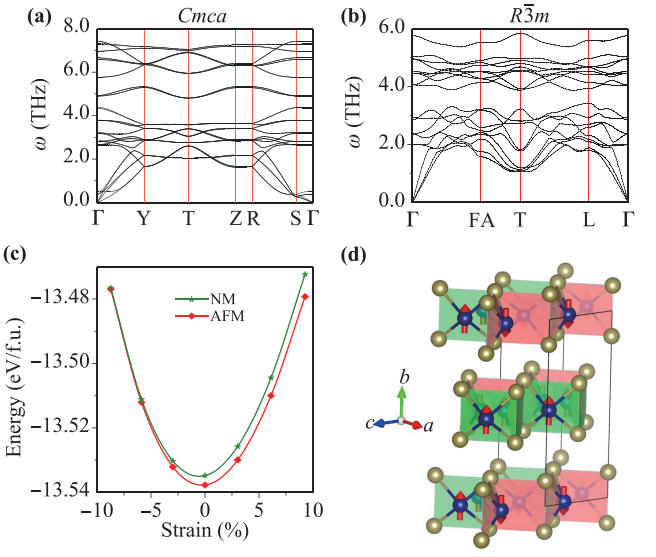

Fig. 3 The phonon spectrums of CrTe in **(a)** $Cmca$ and **(b)** $R\bar{3}m$ structure. **(c)** The total energy of $Cmca$ structure in NM and the most stable AFM state as a function of strain. **(d)** The spin configuration of $Cmca$ phase in the most stable AFM state. The red arrows indicate the direction of the spin of Cr atoms.

stable one [see Fig. 2(a)]. However, in PBE+U calculations, the $P6_3/mmc$ (NA) structure becomes the ground-state structure [see Fig. 2(b)] which is consistent with the available experiments [9, 10]. It was indicated that the electronic correlation effect has to be considered in the investigation of the structures of CrTe. Our results about the ground state of CrTe in PBE and PBE+U calculations are different from previous works [15, 17, 20–22] (see Table S1). Firstly, both the $Cmca$ and $R\bar{3}m$ phases have not been considered in previous works. Secondly, the FP-LAPWs method and MBJ method [15, 20–22] may not be suited for determining the ground state of CrTe. For example, the FP-LAPWs method can not calculate stress tensor, which makes the optimization tedious for low symmetry cases [39]. On the other side, the MBJ method is a potential-only functional and is not suited for computing Hellmann–Feynman forces [40]. In the following content, we will display the results of PBE+U calculations.

The optimized lattice parameters of low-energy CrTe structures are given in Table 1. The phonon spectrums of four low-energy structures show no imaginary phonon frequencies, confirming their dynamical stability [see Figs. 3(a) and (b), and Fig. S2]. Meanwhile, Table 2 lists the elastic constants of the four structures of CrTe, which satisfy the Born criterion [41, 42], indicating that they are mechanically stable. Detailed information about the Born criterion for each phase can be found in Table S2 of the supplementary material.

Two meta-stable structures including $Cmca$ and $R\bar{3}m$ structures were predicted, which were not reported in previous works. The $Cmca$ structure has a layered crystal lattice with each layer be held together by the vdw interaction. Its single layer consists of Cr_4Te_4 cells with four edge-shared $CrTe_4$ quadrangular pyramids [see Fig. 3(d)]. We have compared the energy of $Cmca$ structure in non-magnetic (NM), FM and, different AFM states. It was founded that the FM state was unstable and would change to the NM state. The magnetic ground state of the $Cmca$ phase is the AFM state [see Fig. 3(c)], in which the spin distribution in a single layer is opposite [see Fig. 3(d)]. The AFM state, which helps to decrease the Pauli repulsion between electrons, results in shorter Cr–Te bond lengths than that of other structures (see Table 1). Moreover, the calculated cleaved energy of a single layer is 0.464 J/m^2, similar to that of graphene (0.43 J/m^2) [43], indicating the possible synthesis of monolayer CrTe.

On the other side, the ground state of the $R\bar{3}m$ struc-

Table 2 The independent elastic constants C_{ij} (GPa) for CrTe with various space group: cubic ($Fm\bar{3}m$), hexagonal ($P6_3/mmc$), trigonal ($R\bar{3}m$), and orthorhombic ($Cmca$) phases.

SG	C_{11}	C_{22}	C_{33}	C_{44}	C_{55}	C_{66}	C_{12}	C_{13}	C_{14}	C_{23}
$Cmca$	53.184	37.381	61.232	22.160	34.932	26.810	16.456	24.746		13.526
$P6_3/mmc$	66.858		81.294	3.891			58.537	40.015		
$R\bar{3}m$	77.804		77.033	23.907			39.082	41.394	–2.418	
$Fm\bar{3}m$	119.567			16.885			21.870			

ture is the FM state. The AFM state energy is 195.58 meV/f.u. higher than the FM state, similar to $Fm\bar{3}m$ and $P6_3/mmc$ structure (see Fig. S3). The basic unit of $R\bar{3}m$ structure is the octahedron, similar to $Fm\bar{3}m$ and $P6_3/mmc$ structure (see Fig. S4). As seen from Fig. 2, in both PBE and PBE+U calculations, the energy of $R\bar{3}m$ structure is slightly higher than that of $P6_3/mmc$ (NA) structure, but lower than $Fm\bar{3}m$ (RS) structures as well as ZB structures. Thus, it was possible to synthesize the $R\bar{3}m$ structure in future experiments.

3.2 Electronic and magnetic properties

As shown in Fig. S5, the charge density difference of CrTe in various structures indicates that electrons are transferred from Cr atoms to the middle zone of Cr–Te bonds, which indicates a mixture of ionic and covalent bonding interactions between Cr and Te atoms [44]. The Cr–Te bond lengths (d_{Cr-Te}) of $P6_3/mmc$, $R\bar{3}m$, and $Fm\bar{3}m$ structures is longer than that of the $Cmca$ phase (see Table 1). The extension of d_{Cr-Te} leads to a decrease in covalent bond interaction, contrary to the ionic bonding interaction [20]. Therefore, the unpaired electrons accumulated on the Cr and Te atoms in CrTe of these three structures slightly increase compared to $Cmca$ structure, leading to a variation of magnetism.

Figure 4 shows spin-dependent band structure and partial density of states (DOS) of the $Cmca$ and $R\bar{3}m$ structure with $U_f = 4.0$ eV at its equilibrium volume. The $Cmca$ structure is an AFM metal which indicates the possible existence of giant magnetoresistance [2]. On the other side, $R\bar{3}m$ is a FM half-metal with 100% spin-polarized carrier at Fermi level. The DOS near the Fermi level is mainly from the Cr-3d orbitals in both phases (see Fig. 4). The analysis of crystal orbital hamilton populations (–COHP) shows that the DOS near the Fermi level consist of anti-bonding states between Cr-3d and Te-5p orbitals (see Fig. S6). Here, we founded that the electron correlation effect has a large influence on the electronic structure of CrTe. For example, the $Cmca$ structure become an AFM semiconductor with a bandgap of 0.126 eV if U_f of Cr was ignored (see Fig. S7).

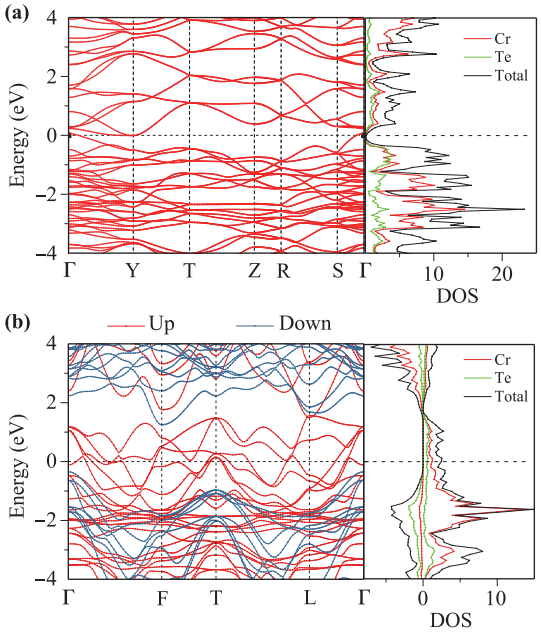

Fig. 4 The spin-dependent band structure and partial density of states (DOS) of CrTe in **(a)** $Cmca$ and **(b)** $R\bar{3}m$ phases.

3.3 Magnetic and structural phase diagram under pressure

We next implored the evolution of the stable structure and phase transition of CrTe as a function of external pressure. Figure 5 plots the pressure-formation enthalpies curve of the CrTe in various structures. We set the formation enthalpies of $P6_3/mmc$ phase to zero for a comparison.

As seen from Fig. 5, the $P6_3/mmc$ structure was found to be the most stable phase at a range of 0 ∼ 34 GPa. However, the energy differences among $P6_3/mmc$, $R\bar{3}m$, and $Fm\bar{3}m$ structures are small. At a range of 30 ∼ 45 GPa, pressure-induced phase transitions occur. The $P6_3/mmc$ structure transforms to the $R\bar{3}m$ structure at 34 GPa and then to $Fm\bar{3}m$ structure at 42 GPa. Here the transition critical pressures were estimated by linear interpolation. During the phase transition, CrTe becomes a FM metal (see Fig. S8). We also checked the MnP-type CrTe (space group $Pnma$) which was also observed in the experiment [13]. We predicted that $Pnma$ structure has higher formation enthalpy than $R\bar{3}m$ and $Fm\bar{3}m$ structures at high pressure (see Fig. 5). Thus, the high-pressure phase of CrTe should be $R\bar{3}m$ and $Fm\bar{3}m$ structures. Thus, the high-pressure phase of CrTe should be $R\bar{3}m$ and $Fm\bar{3}m$ structures. The pressure-induced phase transition path is given below [45]:

$$P6_3/mmc \xrightarrow{34\text{GPa}} R\bar{3}m \xrightarrow{42\text{GPa}} Fm\bar{3}m. \quad (2)$$

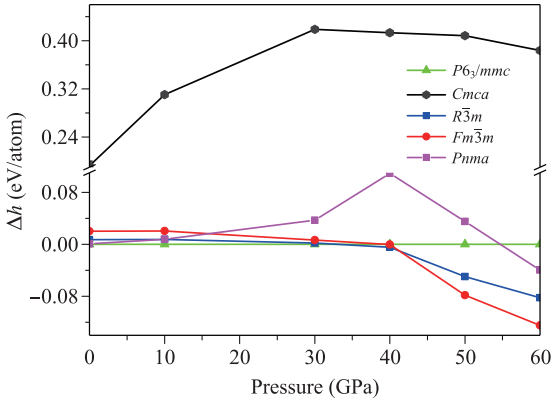

Fig. 5 The relative formation enthalpy of the CrTe in $Cmca$, $R\bar{3}m$, $Fm\bar{3}m$ and $Pmna$ structure with respect to that of the $P6_3/mmc$ structure as a function of pressure.

4 Conclusion

In conclusion, we investigated the crystal structures and magnetic properties of CrTe by using particle swarm optimization algorithm combined with the first-principles calculations. It is necessary to consider the electronic correlation effect in determining the ground state of CrTe. The ground state of CrTe was founded to be the NiAs-type (space group $P6_3/mmc$) structure at ambient pressure, consistent with available experiments. Apart from that, we predicted two meta-stable phases including $Cmca$ and $R\bar{3}m$ structures. CrTe in $Cmca$ structures is a layered AFM metal. CrTe in $R\bar{3}m$ structures is a FM half-metal and may be synthesized in the future experiment, due to that its energy is slightly higher than ground-state $P6_3/mmc$ structure at ambient pressure. The CrTe in $P6_3/mmc$ structure is the most stable at low pressure. However, the ground-state structure of CrTe would transition to $R\bar{3}m$ and $Fm\bar{3}m$ structures at the pressure of about 34 and 42 GPa, respectively. Meanwhile, CrTe becomes a FM metal at high pressure.

Electronic supplementary material See the supplemental material for the estimation of effective onsite U_f value; the phonon dispersion of CrTe; the energy-volume curve of CrTe in $R\bar{3}m$ structures; the energy difference between the lowest-energy antiferromagnetic state and ground-state ferromagnetic state; the charge density difference of CrTe; the crystal orbital hamilton populations (–COHP) of CrTe; the band structure of CrTe in high pressure; the convex hull of Cr–Te compounds with different chemical compositions; the comparing of ground state of CrTe in previous works; the independent elastic constant and Born criterion of CrTe structure. They are available in the online version of this article at https://doi.org/10.1007/s11467-020-1088-3 and http://journal.hep.com.cn/fop/10.1007/s11467-020-1088-3 and are accessible for authorized users.

Acknowledgements This work was supported by the National Natural Science Foundation of China (Nos. 11904312 and 11904313), the Project of Hebei Educational Department, China (Nos. ZD2018015 and QN2018012), the Natural Science Foundation of Hebei Province of China (No. A2020203027), the Doctor Foundation Project of Yanshan University (No. BL19008), and the Scientific Research Foundation of the Higher Education of Hebei Province, China (No. BJ2020015). The numerical calculations in this paper have been done on the supercomputing system in the High Performance Computing Center of Yanshan University.

References

1. A. Brataas, A. D. Kent, and H. Ohno, Current-induced torques in magnetic materials, *Nat. Mater.* 11(5), 372 (2012)
2. A. S. Núñez, R. A. Duine, P. Haney, and A. H. MacDonald, Theory of spin torques and giant magnetoresistance in antiferromagnetic metals, *Phys. Rev. B* 73(21), 214426 (2006)
3. B. G. Park, J. Wunderlich, X. Martí, V. Holý, Y. Kurosaki, M. Yamada, H. Yamamoto, A. Nishide, J. Hayakawa, H. Takahashi, A. B. Shick, and T. Jungwirth, A spin-valve-like magnetoresistance of an antiferromagnet-based tunnel junction, *Nat. Mater.* 10(5), 347 (2011)
4. E. V. Gomonay and V. M. Loktev, Spintronics of antiferromagnetic systems, *Low Temp. Phys.* 40(1), 17 (2014)
5. Y. Wang, C. Song, J. Zhang, and F. Pan, Spintronic materials and devices based on antiferromagnetic metals, *Prog. Nat. Sci.* 27(2), 208 (2017)
6. N. V. Baranov, N. V. Selezneva, and V. A. Kazantsev, Magnetism and superconductivity of transition metal chalcogenides, *Phys. Met. Metallogr.* 119(13), 1301 (2018)
7. W. Zhang, P. K. J. Wong, R. Chua, and A. T. S. Wee, in: Spintronic 2D Materials, Materials Today, edited by W. Liu and Y. Xu, Elsevier, 2020, pp 227–251
8. M. A. Mc Guire, Cleavable magnetic materials from van der Waals layered transition metal halides and chalcogenides, *J. Appl. Phys.* 128(11), 110901 (2020)
9. H. Ipser, K. L. Komarek, and K. O. Klepp, Transition metal-chalcogen systems viii: The Cr–Te phase diagram, *J. Less Common Met.* 92(2), 265 (1983)
10. T. Kanomata, Y. Sugawara, T. Kaneko, K. Kamishima, H. Aruga Katori, and T. Goto, Giant magnetovolume effect of CrTe, *J. Alloys Compd.* 297(1–2), 5 (2000)
11. M. Wang, L. Kang, J. Su, L. Zhang, H. Dai, H. Cheng, X. Han, T. Zhai, Z. Liu, and J. Han, Two-dimensional ferromagnetism in CrTe flakes down to atomically thin layers, *Nanoscale* 12(31), 16427 (2020)
12. M. G. Sreenivasan, J. F. Bi, K. L. Teo, and T. Liew, Systematic investigation of structural and magnetic properties in molecular beam epitaxial growth of metastable zinc-blende CrTe toward half-metallicity, *J. Appl. Phys.* 103(4), 043908 (2008)
13. T. Eto, M. Ishizuka, S. Endo, T. Kanomata, and T. Kikegawa, Pressure-induced structural phase transition in a ferromagnet CrTe, *J. Alloys Compd.* 315(1–2), 16 (2001)
14. M. A. Mc Guire, V. O. Garlea, S. Kc, V. R. Cooper, J. Yan, H. Cao, and B. C. Sales, Antiferromagnetism in the van der Waals layered spin-lozenge semiconductor $CrTe_3$, *Phys. Rev. B* 95(14), 144421 (2017)
15. Z. Charifi, D. Guendouz, H. Baaziz, F. Soyalp, and B. Hamad, *Ab-initio* investigations of the structural, electronic, magnetic and mechanical properties of CrX (X = As, Sb, Se, and Te) transition metal pnictides and chalcogenides, *Phys. Scr.* 94(1), 015701 (2019)
16. J. Dijkstra, H. H. Weitering, C. F. Bruggen, C. Haas, and R. A. Groot, Band-structure calculations, and magnetic and transport properties of ferromagnetic chromium tellurides (CrTe, Cr_3Te_4, Cr_2Te_3), *J. Phys.: Condens. Matter* 1(46), 9141 (1989)
17. V. Kanchana, G. Vaitheeswaran, and M. Rajagopalan, Pressure-induced structural and magnetic phase transition in ferromagnetic CrTe, *J. Magn. Magn. Mater.* 250, 353 (2002)

18. W. H. Xie, Y. Q. Xu, B. G. Liu, and D. G. Pettifor, Half-metallic ferromagnetism and structural stability of zincblende phases of the transition-metal chalcogenides, *Phys. Rev. Lett.* 91(3), 037204 (2003)
19. T. Block and W. Tremel, Large magnetoresistance at room temperature in the off-stochiometric chalcogenide $Cr_{0.92}Te$, *J. Alloys Compd.* 422(1–2), 12 (2006)
20. Y. Liu, S. K. Bose, and J. Kudrnovský, First-principles theoretical studies of half-metallic ferromagnetism in CrTe, *Phys. Rev. B* 82(9), 094435 (2010)
21. A. Belkadi, K. O. Obodo, Y. Zaoui, H. Moulkhalwa, L. Beldi, and B. Bouhafs, First-principles studies of structural, electronic and magnetic properties of the CrS, CrSe and CrTe compounds, *SPIN* 08(04), 1850019 (2018)
22. H. Moulkhalwa, Y. Zaoui, K. O. Obodo, A. Belkadi, L. Beldi, and B. Bouhafs, Half-metallic and half-semiconductor gaps in Cr-based chalcogenides: DFT+U calculations, *J. Supercond. Nov. Magn.* 32(3), 635 (2019)
23. Y. Wang, J. Lv, L. Zhu, and Y. Ma, CALYPSO: A method for crystal structure prediction, *Comput. Phys. Commun.* 183(10), 2063 (2012)
24. Y. Wang, J. Lv, L. Zhu, and Y. Ma, Crystal structure prediction via particle-swarm optimization, *Phys. Rev. B* 82(9), 094116 (2010)
25. B. Gao, P. Gao, S. Lu, J. Lv, Y. Wang, and Y. Ma, Interface structure prediction via CALYPSO method, *Sci. Bull. (Beijing)* 64(5), 301 (2019)
26. A. P. Drozdov, M. I. Eremets, I. A. Troyan, V. Ksenofontov, and S. I. Shylin, Conventional superconductivity at 203 kelvin at high pressures in the sulfur hydride system, *Nature* 525(7567), 73 (2015)
27. F. Peng, Y. Sun, C. J. Pickard, R. J. Needs, Q. Wu, and Y. Ma, Hydrogen clathrate structures in rare earth hydrides at high pressures: Possible route to room-temperature superconductivity, *Phys. Rev. Lett.* 119(10), 107001 (2017)
28. Y. Nishihara, Y. Yamaguchi, M. Tokumoto, K. Takeda, and K. Fukamichi, Superconductivity and magnetism of bcc Cr–Ru alloys, *Phys. Rev. B* 34(5), 3446 (1986)
29. A. J. Bradley, The crystal structures of the rhombohedral forms of selenium and tellurium, *Lond. Edinb. Dublin Philos. Mag. J. Sci.* 48(285), 477 (2009)
30. G. Kresse and J. Furthmüller, Efficient iterative schemes for *ab initio* total-energy calculations using a plane-wave basis set, *Phys. Rev. B* 54(16), 11169 (1996)
31. G. Kresse and D. Joubert, From ultrasoft pseudopotentials to the projector augmented-wave method, *Phys. Rev. B* 59(3), 1758 (1999)
32. P. E. Blöchl, Projector augmented-wave method, *Phys. Rev. B* 50(24), 17953 (1994)
33. J. P. Perdew, K. Burke, and M. Ernzerhof, Generalized gradient approximation made simple, *Phys. Rev. Lett.* 77(18), 3865 (1996)
34. H. J. Monkhorst and J. D. Pack, Special points for Brillouin-zone integrations, *Phys. Rev. B* 13(12), 5188 (1976)
35. W. E. Pickett, S. C. Erwin, and E. C. Ethridge, Reformulation of the LDA+U method for a local-orbital basis, *Phys. Rev. B* 58(3), 1201 (1998)
36. M. Cococcioni and S. de Gironcoli, Linear response approach to the calculation of the effective interaction parameters in the LDA+U method, *Phys. Rev. B* 71(3), 035105 (2005)
37. A. Togo and I. Tanaka, First principles phonon calculations in materials science, *Scr. Mater.* 108, 1 (2015)
38. S. Grimme, Semiempirical GGA-type density functional constructed with a long-range dispersion correction, *J. Comput. Chem.* 27(15), 1787 (2006)
39. P. Blaha, K. Schwarz, F. Tran, R. Laskowski, G. K. H. Madsen, and L. D. Marks, WIEN2k: An APW+LO program for calculating the properties of solids, *J. Chem. Phys.* 152(7), 074101 (2020)
40. K. Choudhary, Q. Zhang, A. C. Reid, S. Chowdhury, N. Van Nguyen, Z. Trautt, M. W. Newrock, F. Y. Congo, and F. Tavazza, Computational screening of high-performance optoelectronic materials using OptB88vdW and TB-mBJ formalisms, *Sci. Data* 5(1), 180082 (2018)
41. F. Mouhat and F. X. Coudert, Necessary and sufficient elastic stability conditions in various crystal systems, *Phys. Rev. B* 90(22), 224104 (2014)
42. Z. J. Wu, E. J. Zhao, H. P. Xiang, X. F. Hao, X. J. Liu, and J. Meng, Crystal structures and elastic properties of superhard IrN_2 and IrN_3 from first principles, *Phys. Rev. B* 76(5), 054115 (2007)
43. T. Björkman, A. Gulans, A. V. Krasheninnikov, and R. M. Nieminen, van der Waals bonding in layered compounds from advanced density-functional first-principles calculations, *Phys. Rev. Lett.* 108(23), 235502 (2012)
44. K. Nakada, H. Shimizu, and H. Yamada, Electronic structure and magnetism of CrTe with NiAs-type structure, *J. Magn. Magn. Mater.* 272–276, 464 (2004)
45. I. Benabdelkader, H. Bendaoud, K. O. Obodo, L. Beldi, and B. Bouhafs, An *ab initio* study on the transition path of carbon dioxide at high pressure: Evidence for a new intermediate $P\bar{4}m2$ phase, *Comput. Condens. Matter* 21, e00429 (2019)